

# BLACK HOLE SHADOW OF SGR A\* IN DARK MATTER HALO

XIAN HOU,<sup>1,2,3</sup> ZHAOYI XU,<sup>1,2,3,4</sup> MING ZHOU,<sup>1,2,3</sup> JIANCHENG WANG<sup>1,2,3,4</sup>

<sup>1</sup>Yunnan Observatories, Chinese Academy of Sciences, 396 Yangfangwang, Guandu District, Kunming, 650216, P. R. China; xianhou.astro@gmail.com, zyxu88@ynao.ac.cn

<sup>2</sup>Key Laboratory for the Structure and Evolution of Celestial Objects, Chinese Academy of Sciences, 396 Yangfangwang, Guandu District, Kunming, 650216, P. R. China

<sup>3</sup>Center for Astronomical Mega-Science, Chinese Academy of Sciences, 20A Datun Road, Chaoyang District, Beijing, 100012, P. R. China

<sup>4</sup>University of Chinese Academy of Sciences, Beijing, 100049, P. R. China

## ABSTRACT

We study, for the first time, the shadow of the supermassive black hole Sgr A\* at the center of the Milky Way in dark matter halos. For the Cold Dark Matter and Scalar Field Dark Matter models considered in this work, the apparent shape of the shadow depends upon the black hole spin  $a$  and the dark matter parameter  $k$ . We find that both dark matter models influence the shadow in a similar way. The shadow is a perfect circle in the non-rotating case ( $a = 0$ ) and a deformed one in the rotating case ( $a \neq 0$ ). The size of the shadow increases with increasing  $k$  in both non-rotating and rotating cases, while the shadow gets more and more distorted with increasing  $a$  in the rotating case. We further investigate the black hole emission rate in both dark matter halos. We find that the emission rate decreases with increasing  $k$  and the peak of the emission shifts to lower frequency. Finally, by calculating the angular radius of the shadow, we estimate that the dark matter halo could influence the shadow of Sgr A\* at a level of order of magnitude of  $10^{-3} \mu\text{as}$  and  $10^{-5} \mu\text{as}$ , for CDM and SFDM, respectively. Future astronomical instruments with high angular resolution would be able to observe this effect and shed light on the nature of Sgr A\*. More interestingly, it may be possible to distinguish between CDM and SFDM models given the resolutions required differing by two orders of magnitude from each other.

*Keywords:* Dark matter, Black hole shadow, Sgr A\*

## 1. INTRODUCTION

It is widely believed that the center of our own galaxy, the Milky Way, hosts a supermassive black hole Sgr A\*. One of the ways to prove the existence of a black hole is to observe its shadow, which is the optical appearance cast by the black hole and appears as a two-dimensional dark zone for the observer on Earth. The black hole shadow can provide us information on fundamental properties of the black hole, i.e., the mass and the spin, thus enable a direct probe of the immediate environment of a black hole and the dynamics near the black hole. This will eventually serves as a test of fundamental predictions of Einstein's theory of General Relativity (GR). First images of the black hole Sgr A\* at the center of the Milky Way and the black hole M87 at the center of the Virgo A galaxy are expected to be obtained using the sub-millimeter "Event Horizon Telescope" (EHT)<sup>1</sup> (Doeleman et al. 2008) based on the very-long baseline interferometry (VLBI).

The shadow of the Schwarzschild black hole was first discussed by Synge (1966) and later by Lunin (1979) who considered the effect of a thin accretion disk on the shadow. Bardeen (1973) was the first to study the shadow cast by the Kerr black hole. Through constructing two observables, Hioki and Maeda Hioki & Maeda (2009) examined the shadow of the Kerr black hole or a Kerr naked singularity. This topic has been extended to other black hole space-time by various researchers, e.g., Kerr-Newman black hole (de Vries 2000; Takahashi 2005; Tsukamoto 2018), Einstein-Maxwell-Dilation-Axion black hole (Wei & Liu 2013), Kerr-Taub-NUT black hole (Abdujabbarov et al. 2013), Braneworld black hole (Schee & Stuchlík 2009; Amarilla & Eiroa 2012), Kaluza-Klein rotating dilation black hole (Amarilla & Eiroa 2013), non-Kerr black hole (e.g., Bambi et al. 2012; Atamurotov et al. 2013; Wang et al. 2017), Tomimatsu-Sato black hole (Bambi & Yoshida 2010), Johannsen-Psaltis black hole (Younsi et al. 2016), Einstein-

<sup>1</sup> www.Eventhorizontelescope.org.

dilaton-Gauss-Bonnet black hole (Younsi et al. 2016; Cunha et al. 2017), Kerr-Sen black hole (Dastan et al. 2016; Younsi et al. 2016), regular black holes (e.g., Abdujabbarov et al. 2016), nonsingular black holes (e.g., Amir & Ghosh 2016), Ayón Beato García black hole (Saha et al. 2018), black hole with cosmological constant (Grenzbach et al. 2014; Perlick et al. 2018; Eiroa & Sendra 2018), etc. Multiple shadows of a single black hole have also been discussed recently (e.g., Cunha et al. 2015; Grover et al. 2018), as well as the shadow of multiple black holes (Yumoto et al. 2012; Cunha et al. 2018). The black hole shadow in modified GR has also been investigated in the literature, e.g., in extended Chern-Simons modified gravity (Amarilla et al. 2010), in Rastall gravity (Kumar et al. 2017), in Vector-Tensor Galileons Modified Gravity (Vetsov et al. 2018), in fourth-order conformal Weyl gravity (Mureika & Varieschi 2017), etc. In addition, the study of shadow has been extended to black holes with higher or extra dimensions (e.g., Papnoi et al. 2014; Abdujabbarov et al. 2015; Amir et al. 2017; Pratap Singh & Ghosh 2017) and black holes surrounded by plasma (e.g., Atamurotov et al. 2015; Perlick et al. 2015). Specific attentions have been paid to the black hole Sgr A\* using analytical approach and magnetohydrodynamic simulations considering more realistic situations with accretion flow and relativistic jets. The results have been compared with the EHT observations of Sgr A\* to constrain the accretion and jet models (e.g., Falcke et al. 2000; Noble et al. 2007; Dexter et al. 2010; Mościbrodzka et al. 2014; Chan et al. 2015; Broderick et al. 2016; Gold et al. 2017). The possibility of testing theories of gravity basing on the shadow of Sgr A\* has been equally discussed by various authors (e.g., Broderick & Loeb 2006; Bambi & Freese 2009; Broderick et al. 2014; Psaltis et al. 2015; Johannsen et al. 2016; Mizuno et al. 2018). A review of the black hole shadow can be referred to Cunha & Herdeiro (2018).

On the other hand, according to the Standard Model of cosmology, the Universe is composed mostly of dark matter (27%) and dark energy (68%), while baryonic matter contributes only 5% to the total mass-energy of the Universe. It is therefore natural to study the black hole shadow in the presence of dark energy and dark matter. Recently, Pratap Singh (2017) and Abdujabbarov et al. (2017) studied the black hole shadow in quintessence. Given that in galactic scale or near the black hole, the gravitational effect of dark matter is larger than dark energy, the influence of dark matter on the black hole properties might be equally more significant than dark energy. Thus, it is of greater interest to study the black hole shadow in dark matter halo.

Though no direct measurements have been made of the particle nature of dark matter, observational evidences supporting the existence of dark matter are accumulating through measurements of, for example, galactic rotation curves (Rubin et al. 1980), galaxy cluster dynamics (Zwicky 1933), the cosmic microwave background (Planck Collaboration et al. 2014), the primordial abundances of heavy isotopes produced by big bang nucleosynthesis (Olive 2003), etc. Among various theoretical dark matter models developed to explain the observations, Cold Dark Matter model (CDM) (Navarro et al. 1996, 1997; Dubinski & Carlberg 1991) is the current most popular one which shows excellent consistency between observations and numerical simulations of large-scale structure of the Universe. However, strong tension exists between long-standing (and more recent) small-scale structure observations (Tulin & Yu 2018) and CDM model predictions. Alternative models, such as Scalar Field Dark Matter model (SFDM) (e.g., Spergel & Steinhardt 2000; Ureña-López et al. 2002; Harko 2011), have been proposed. In particular, SFDM model can successfully, on the one hand, solve the small-scale structure problems and, on the other hand, keep great concordance with large-scale structure observations.

A leading class of the dark matter particle candidates is Weakly Interacting Massive Particles (WIMPs), which are predicted to produce observable gamma rays, cosmic rays, and neutrinos through annihilations or decays. The Galactic center of the Milky Way, due to its proximity and high dark matter density, is expected to be the brightest dark matter source on the sky. Evidence of annihilation signal of WIMPs from the Galactic center has been arising in the past decade from gamma-ray observations with space and ground-based telescopes like *Fermi*-LAT and H.E.S.S (See Cirelli 2015, for a review on this topic). In this context, our work will, for the first time, investigate the shadow cast by the black hole Sgr A\* at the Galactic center in dark matter halos.

The paper is organized as follows. In Section 2, we introduce the space-time metric for spherical symmetric and rotating black hole in the two kinds of dark matter halos. In Section 3, we derive the complete null geodesic equations and the motion of a test particle in the rotating black hole space-time. In Section 4, we study the apparent shapes of the shadow cast by the black hole Sgr A\* in the presence of two kinds of dark matter halos. The energy emission rate of the black hole Sgr A\* is investigated in Section 5 and we discuss our results in Section 6.

## 2. BLACK HOLE SPACE-TIME IN DARK MATTER HALO

### 2.1. Spherical symmetric black hole in dark matter halo

The spherical symmetric black hole space-time metric in dark matter halo is (Xu et al. 2018, and references therein)

$$ds^2 = -f(r)dt^2 + \frac{dr^2}{f(r)} + r^2(d\theta^2 + \sin^2\theta d\phi^2). \quad (1)$$

For CDM halo:

$$f(r) = \left(1 + \frac{r}{\tilde{R}}\right)^{-\frac{8\pi G\rho_c \tilde{R}^3}{c^2 r}} - \frac{2GM}{rc^2}, \quad (2)$$

where  $M$  is the black hole mass,  $c$  is the light of speed,  $\rho_c$  is the density of the universe at the moment when the dark matter halo collapsed and  $\tilde{R}$  is the characteristic radius.

For SFDM halo:

$$f(r) = \exp\left[-\frac{8G\rho_c R^2}{\pi} \frac{\sin(\pi r/R)}{\pi r/R}\right] - \frac{2GM}{rc^2}, \quad (3)$$

where  $\rho_c$  is the central density and  $R$  is the radius at which the pressure and density are zero.

When there is no dark matter halo ( $\rho_c = 0$ ), the above metrics reduce to that of the Schwarzschild black hole.

### 2.2. Rotating black hole in dark matter halo

The rotating black hole space-time metric in dark matter halo is (Xu et al. 2018)

$$ds^2 = -\left(1 - \frac{r^2 - f(r)r^2}{\Sigma^2}\right) dt^2 + \frac{\Sigma^2}{\Delta} dr^2 + \frac{2(r^2 - f(r)r^2)a\sin^2\theta}{\Sigma^2} d\phi dt + \Sigma^2 d\theta^2 + \frac{\sin^2\theta}{\Sigma^2} ((r^2 + a^2)^2 - a^2 \Delta \sin^2\theta) d\phi^2, \quad (4)$$

where

$$\Sigma^2 = r^2 + a^2 \cos^2\theta, \quad (5)$$

$$\Delta = r^2 f(r) + a^2, \quad (6)$$

and  $f(r)$  takes the same form as Eq. (2) and Eq. (3) for CDM and SFDM, respectively. Below we give the explicit expressions of the space-time metric for CDM halo and SFDM halo.

For CDM halo:

$$ds^2 = -\left[1 - \frac{r^2 + \frac{2GMr}{c^2} - r^2 \left(1 + \frac{r}{\tilde{R}}\right)^{-\frac{8\pi G\rho_c \tilde{R}^3}{c^2 r}}}{\Sigma^2}\right] dt^2 + \frac{\Sigma^2}{\Delta} dr^2 + \Sigma^2 d\theta^2 + \frac{\sin^2\theta}{\Sigma^2} ((r^2 + a^2)^2 - a^2 \Delta \sin^2\theta) d\phi^2 + \frac{2 \left[ r^2 + \frac{2GMr}{c^2} - r^2 \left(1 + \frac{r}{\tilde{R}}\right)^{-\frac{8\pi G\rho_c \tilde{R}^3}{c^2 r}} \right] a \sin^2\theta}{\Sigma^2} d\phi dt, \quad (7)$$

where

$$\Delta = r^2 \left(1 + \frac{r}{\tilde{R}}\right)^{-\frac{8\pi G\rho_c \tilde{R}^3}{c^2 r}} - \frac{2GMr}{c^2} + a^2. \quad (8)$$

For SFDM halo:

$$ds^2 = -\left[1 - \frac{r^2 + \frac{2GMr}{c^2} - r^2 \exp\left(-\frac{8G\rho_c R^2}{\pi} \frac{\sin(\pi r/R)}{\pi r/R}\right)}{\Sigma^2}\right] dt^2 + \frac{\Sigma^2}{\Delta} dr^2 + \Sigma^2 d\theta^2$$

$$+ \frac{2 \left[ r^2 + \frac{2GMr}{c^2} - r^2 \exp \left( -\frac{8G\rho_c R^2 \sin(\pi r/R)}{\pi} \right) \right] a \sin^2 \theta}{\Sigma^2} d\phi dt + \frac{\sin^2 \theta}{\Sigma^2} ((r^2 + a^2)^2 - a^2 \Delta \sin^2 \theta) d\phi^2, \quad (9)$$

where

$$\Delta = r^2 \exp \left[ -\frac{8G\rho_c R^2 \sin(\pi r/R)}{\pi} \right] - \frac{2GMr}{c^2} + a^2. \quad (10)$$

In this work, we set  $G = 1$  and  $c = 1$ . Furthermore, we define  $k = \rho_c \tilde{R}^3$  and  $k = \rho_c R^3$ , for CDM halo and SFDM halo, respectively, to stand for the dark matter amount. For the black hole Sgr A\*, we adopt the values of different parameters reported in [de Oliveira et al. \(2015\)](#). For CDM halo,  $\rho_c = 1.936 \times 10^7 \text{ M}_\odot \text{ kpc}^{-3}$  and  $\tilde{R} = 17.46 \text{ kpc}$ . For SFDM halo,  $\rho_c = 3.43 \times 10^7 \text{ M}_\odot \text{ kpc}^{-3}$  and  $R = 15.7 \text{ kpc}$ . We then obtain  $k = 23965$  and  $k = 30869$  in unit of the mass of Sgr A\* ( $4.3 \times 10^6 \text{ M}_\odot$ ), for CDM and SFDM, respectively. When the dark matter halo is absent ( $\rho_c = 0$  or  $k = 0$  equivalently), the above metrics reduce to that of the general Kerr black hole.

### 3. NULL GEODESICS

Before studying the black hole shadow, it is necessary to first obtain the geodesic structure of a test particle for the above space-time metrics. For this, we employ the Hamilton-Jacobi equation and Carter constant separable method ([Carter 1968](#)). The Hamilton-Jacobi equation takes the general form as

$$\frac{\partial S}{\partial \sigma} = -\frac{1}{2} g^{\mu\nu} \frac{\partial S}{\partial x^\mu} \frac{\partial S}{\partial x^\nu} \quad (11)$$

where  $S$  is the Jacobi action and  $\sigma$  is an affine parameter along the geodesics. The separable solution of the Jacobi action  $S$  reads as

$$S = \frac{1}{2} m^2 \sigma - Et + L\phi + S_r(r) + S_\theta(\theta) \quad (12)$$

where  $m$ ,  $E$  and  $L$  are, respectively, the test particle's mass, energy and angular momentum, with respect to the rotation axis.  $S_r(r)$  and  $S_\theta(\theta)$  are functions of  $r$  and  $\theta$ , respectively. Inserting Eq. (12) into Eq. (11) and applying the variable separable method, we obtain the null geodesic equations for a test particle around the rotating black hole in dark matter halo as

$$\Sigma \frac{dt}{d\sigma} = \frac{r^2 + a^2}{\Delta} [E(r^2 + a^2) - aL] - a(aE \sin^2 \theta - L), \quad (13)$$

$$\Sigma \frac{dr}{d\sigma} = \sqrt{\mathcal{R}}, \quad (14)$$

$$\Sigma \frac{d\theta}{d\sigma} = \sqrt{\Theta}, \quad (15)$$

$$\Sigma \frac{d\phi}{d\sigma} = \frac{a}{\Delta} [E(r^2 + a^2) - aL] - \left( aE - \frac{L}{\sin^2 \theta} \right), \quad (16)$$

where  $\mathcal{R}(r)$  and  $\Theta(\theta)$  take the following form

$$\mathcal{R}(r) = [E(r^2 + a^2) - aL]^2 - \Delta [m^2 r^2 + (aE - L)^2 + \mathcal{K}], \quad (17)$$

$$\Theta(\theta) = \mathcal{K} - \left( \frac{L^2}{\sin^2 \theta} - a^2 E^2 \right) \cos^2 \theta, \quad (18)$$

with  $\mathcal{K}$  the Carter constant. The above geodesic equations (13-16) fully describe the dynamics of the test particle around the rotating black hole in dark matter halo. The boundary of the black hole shadow is mainly determined by the unstable circular orbit. We consider the case of photons and an observer at the infinity which implies that  $m = 0$  and photons arrive near the equatorial plane ( $\theta = \pi/2$ ). The unstable circular orbit satisfies the condition

$$\mathcal{R} = \frac{\partial \mathcal{R}}{\partial r} = 0. \quad (19)$$

Hence, from Eq. (17) and by introducing two impact parameters  $\xi$  and  $\eta$

$$\xi = L/E, \quad \eta = \mathcal{K}/E^2, \quad (20)$$

we obtain

$$(r^2 + a^2 - a\xi)^2 - [\eta + (\xi - a)^2](r^2 f(r) + a^2) = 0, \quad (21)$$

$$4r(r^2 + a^2 - a\xi) - [\eta + (\xi - a)^2](2rf(r) + r^2 f'(r)) = 0. \quad (22)$$

Combining Eqs. (21-22), we get the expressions of  $\xi$  and  $\eta$  as

$$\xi = \frac{(r^2 + a^2)(rf'(r) + 2f(r)) - 4(r^2 f(r) + a^2)}{a(rf'(r) + 2f(r))}, \quad (23)$$

$$\eta = \frac{r^3[8a^2 f'(r) - r(rf'(r) + 2f(r))^2]}{a^2(rf'(r) + 2f(r))^2}. \quad (24)$$

Furthermore, we have

$$\xi^2 + \eta = 2r^2 + a^2 + \frac{16(r^2 f(r) + a^2)}{(rf'(r) + 2f(r))^2} - \frac{8(r^2 f(r) + a^2)}{rf'(r) + 2f(r)} \quad (25)$$

$$= 2r^2 + a^2 + \frac{8\Delta[2 - (rf'(r) + 2f(r))]}{(rf'(r) + 2f(r))^2}. \quad (26)$$

For the CDM halo (Eq. 2), we have

$$f'(r) = \left(1 + \frac{r}{\tilde{R}}\right)^{-\frac{8\pi k}{r}} \left[ \frac{8\pi k}{r^2} \ln \left(1 + \frac{r}{\tilde{R}}\right) - \frac{8\pi k}{r(r + \tilde{R})} \right] + \frac{2M}{r^2}, \quad (27)$$

and then

$$\xi^2 + \eta = 2r^2 + a^2 + \frac{8 \left[ r^2 \left(1 + \frac{r}{\tilde{R}}\right)^{-\frac{8\pi k}{r}} - 2Mr + a^2 \right] \left[ 2 + \frac{2M}{r} - \left(1 + \frac{r}{\tilde{R}}\right)^{-\frac{8\pi k}{r}} \left( \frac{8\pi k}{r} \ln \left(1 + \frac{r}{\tilde{R}}\right) - \frac{8\pi k}{(r + \tilde{R})} + 2 \right) \right]}{\left[ \left(1 + \frac{r}{\tilde{R}}\right)^{-\frac{8\pi k}{r}} \left( \frac{8\pi k}{r} \ln \left(1 + \frac{r}{\tilde{R}}\right) - \frac{8\pi k}{(r + \tilde{R})} + 2 \right) - \frac{2M}{r} \right]^2} \quad (28)$$

Similarly, for the SFDM halo (Eq. 3), we have

$$f'(r) = -\frac{8k}{\pi^2} \left[ \frac{\pi}{Rr} \cos \left( \frac{\pi r}{R} \right) - \frac{1}{r^2} \sin \left( \frac{\pi r}{R} \right) \right] \exp \left[ -\frac{8k}{\pi} \frac{\sin(\pi r/R)}{\pi r} \right] + \frac{2M}{r^2}, \quad (29)$$

and then

$$\xi^2 + \eta = 2r^2 + a^2 + \frac{8 \left[ r^2 \exp \left( -\frac{8k}{\pi} \frac{\sin(\pi r/R)}{\pi r} \right) - 2Mr + a^2 \right] \left[ 2 + \frac{2M}{r} - \left( \frac{8k}{\pi^2 r} \sin \left( \frac{\pi r}{R} \right) - \frac{8k}{\pi R} \cos \left( \frac{\pi r}{R} \right) + 2 \right) \exp \left( -\frac{8k}{\pi} \frac{\sin(\pi r/R)}{\pi r} \right) \right]}{\left[ \left( \frac{8k}{\pi^2 r} \sin \left( \frac{\pi r}{R} \right) - \frac{8k}{\pi R} \cos \left( \frac{\pi r}{R} \right) + 2 \right) \exp \left( -\frac{8k}{\pi} \frac{\sin(\pi r/R)}{\pi r} \right) - \frac{2M}{r} \right]^2} \quad (30)$$

#### 4. BLACK HOLE SHADOW

To determine the shape of the black hole shadow, we introduce the celestial coordinates  $\alpha$  and  $\beta$  as

$$\alpha = \lim_{r_o \rightarrow \infty} \left( -r_o^2 \sin \theta_o \frac{d\phi}{dr} \right), \quad (31)$$

$$\beta = \lim_{r_o \rightarrow \infty} \left( r_o^2 \frac{d\theta}{dr} \right), \quad (32)$$

where  $r_o$  is the distance between the black hole and the observer,  $\theta_o$  is the angle between the rotation axis of the black hole and the line of sight of the observer (i.e., inclination angle). Here we assume the observer is at infinity.  $\alpha$  is the

apparent perpendicular distance of the shadow as seen from the axis of symmetry, and  $\beta$  is the apparent perpendicular distance of the shadow as seen from its projection on the equatorial plane.

Using the null geodesic equations (13-16), we can obtain the relations between celestial coordinates and impact parameters  $\xi$  and  $\eta$  as

$$\alpha = -\frac{\xi}{\sin\theta}, \quad (33)$$

$$\beta = \pm\sqrt{\eta + a^2 \cos^2\theta - \xi^2 \cot^2\theta}. \quad (34)$$

In the equatorial plane ( $\theta = \pi/2$ ),  $\alpha$  and  $\beta$  reduce to

$$\alpha = -\xi, \quad (35)$$

$$\beta = \pm\sqrt{\eta}. \quad (36)$$

By plotting  $\beta$  against  $\alpha$ , we show different shapes of the shadow in Figure 1 and 2, for the CDM halo and SFDM halo, respectively. In the non-rotating case ( $a = 0$ ), the shadow is a perfect circle and the size increases with increasing  $k$ . In the rotating case ( $a \neq 0$ ), the shadow gets more and more distorted for a higher  $a$  given fixed  $k$ , and the size increases with increasing  $k$  given fixed  $a$ , similar to the case of  $a = 0$ . We note that the influence of dark matter on the shadow is actually minor with a visible effect only when  $k$  increases to order of magnitude of  $10^7$ .

From our study, the structure of the black hole shadow in the CDM and SFDM halos is very similar to the cases of Schwarzschild and Kerr black hole. We propose that this is because in our case, the fundamental properties of the black hole is maintained, while the dark matter halo only induces a fluctuation-like effect on the shadow. We can find similar phenomena for black hole shadows in plasma. Yet, if the black hole under study is not Schwarzschild or Kerr black hole, but with extra fundamental parameters, like dilation, or in alternative theories of gravity, the shadow would rather exhibit some obvious dissimilarities. An example of comparison of different black hole shadows can be found in Goddi et al. (2017), Figure 7.

Further study of the black hole shadow relies on two astronomical observables defined in Hioki & Maeda (2009): the radius of the shadow  $R_s$  and the distortion parameter  $\delta_s$ . The schematic illustration of  $R_s$  and  $\delta_s$  is shown in Figure 3.  $R_s$  is the radius of the reference circle passing through three points: the top one  $B(\alpha_t, \beta_t)$ , the bottom one  $D(\alpha_b, \beta_b)$  and the most right one  $A(\alpha_r, 0)$ . The points  $C(\alpha_p, 0)$  and  $F(\tilde{\alpha}_p, 0)$  are where the circle of the shadow and the reference circle cut the horizontal axis at the opposite side of  $A(\alpha_r, 0)$ , respectively.  $d_s$  is the distance from the most left position (C) of the shadow to the reference circle (F).  $R_s$  approximately gives the size of the shadow and  $\delta_s$  measures its deformation with respect to the reference circle. From the geometry of the shadow, we have

$$R_s = \frac{(\alpha_t - \alpha_r)^2 + \beta_t^2}{2|\alpha_r - \alpha_t|}, \quad (37)$$

where we have used the relations  $\alpha_b = \alpha_t$  and  $\beta_b = -\beta_t$ . And

$$\delta_s = \frac{d_s}{R_s} = \frac{|\alpha_p - \tilde{\alpha}_p|}{R_s}. \quad (38)$$

Considering the relation  $\tilde{\alpha}_p = \alpha_r - 2R_s$ , we have

$$\delta_s = 2 - \frac{D_s}{R_s} \quad (39)$$

where  $D_s = \alpha_r - \alpha_p$  is the diameter of the shadow along the axis of  $\alpha$ .

In the non-rotating case ( $a = 0$ ), the shadow of the black hole is a perfect circle with radius of  $R_s$ . So

$$\alpha^2 + \beta^2 = \xi^2 + \eta = R_s^2. \quad (40)$$

Figure 4 and 5 show the variation of the radius  $R_s$  and the distortion parameter  $\delta_s$  with the parameters  $a$  and  $k$  for the CDM halo and SFDM halo, respectively. We find that the radius of the shadow increases with the increasing  $k$ , but almost does not vary with  $a$  (a constant has been added to visualize the trend of  $R_s$  for different  $a$ ). The distortion parameter decreases monotonically with increasing  $k$  for a given  $a$ , and increases with  $a$  for a given  $k$ . This trend could also be inferred from Figure 1 and 2. Similarly, the effect of dark matter is visible only when  $k$  increases to order of magnitude of  $10^7$ .

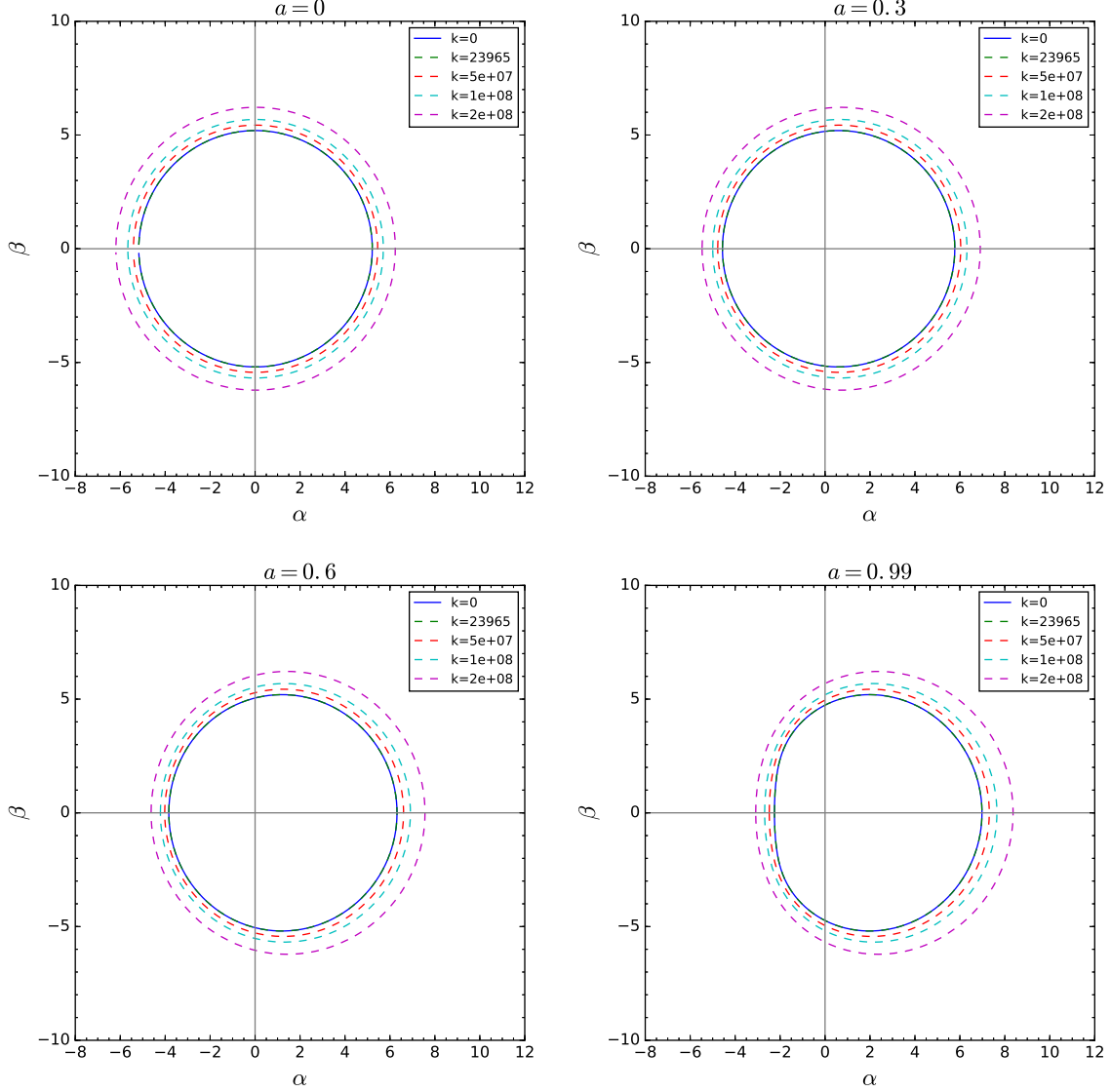


**Figure 1.** Silhouette of the shadow cast by the rotating black hole Sgr A\* in the CDM halo for different values of parameters  $a$  and  $k$ .

## 5. ENERGY EMISSION RATE

For an observer located at an infinite distance, the black hole shadow corresponds to the high energy absorption cross section, the latter oscillating around a limiting constant value  $\sigma_{lim}$  for a spherical symmetric black hole.  $\sigma_{lim}$  is approximately equal to the geometrical cross section of the photon sphere (Mashhoon 1973; Misner et al. 1973) and can be expressed as (Wei & Liu 2013)

$$\sigma_{lim} \approx \pi R_s^2, \quad (41)$$

with  $R_s$  the radius of the black hole shadow. This can be generalized to the rotating black hole considered in this work, given that the shadow approaches to a standard circle as can be seen from Figure 1 and 2. The energy emission rate of the black hole is therefore

$$\frac{d^2 E(\omega)}{d\omega dt} = \frac{2\pi^2 \sigma_{lim}}{e^{\omega/T} - 1} \omega^3 \quad (42)$$

with  $\omega$  the frequency of photon and  $T$  the Hawking temperature for the outer event horizon which is defined by

$$T = \lim_{\theta=0, r \rightarrow r_+} \frac{\partial_r \sqrt{g_{tt}}}{2\pi \sqrt{g_{rr}}}. \quad (43)$$

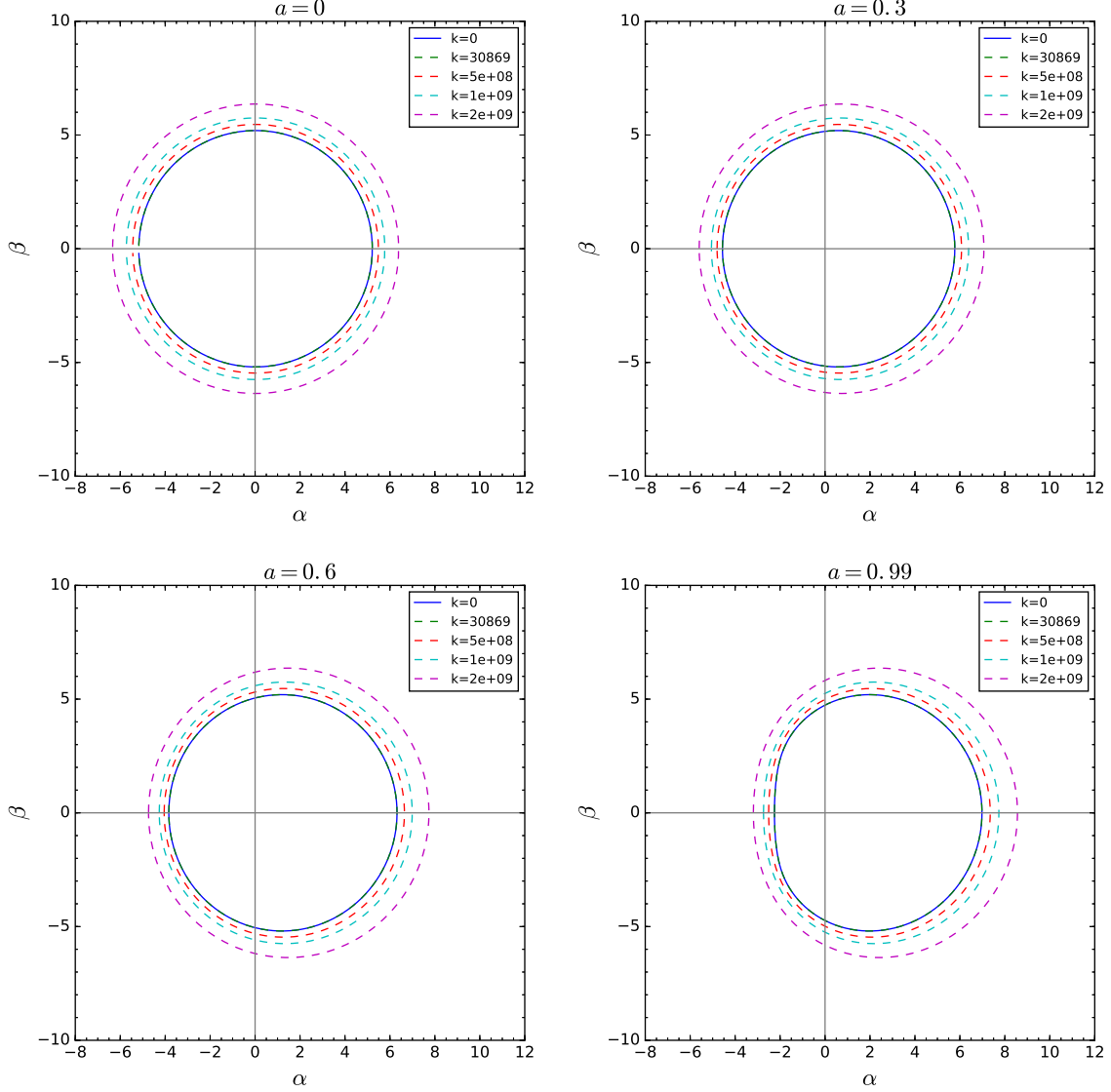


**Figure 2.** Silhouette of the shadow cast by the rotating black hole Sgr A\* in the SFDM halo for different values of parameters  $a$  and  $k$ .

In our case, we have for the rotating black hole in dark matter halo

$$g_{tt} = 1 - \frac{r^2 - f(r)r^2}{\Sigma^2}, \quad g_{rr} = \frac{\Sigma^2}{\Delta}. \quad (44)$$

Thus, we obtain the Hawking temperature as

$$T = \frac{r_+^2 f'(r_+) (r_+^2 + a^2) + 2a^2 r_+ (f(r_+) - 1)}{4\pi(r_+^2 + a^2)^2} \quad (45)$$

where  $r_+$  is the outer event horizon of the black hole defined as the greater root of the solution for  $1/g_{rr} = 0$ .

Eq. (45) reduces to the regular Kerr black hole in the case of  $k = 0$  and takes the form

$$T_{Kerr} = \frac{r_+^2 - a^2}{4\pi r_+ (r_+^2 + a^2)} \quad (46)$$

with  $r_+ = M + \sqrt{M^2 - a^2}$ .

In Figure 6 and 7, we show the energy emission rate against the frequency  $\omega$  for different values of the parameters  $a$  and  $k$ , assuming a CDM halo and SFDM halo, respectively. We can see that the peak of the emission decreases



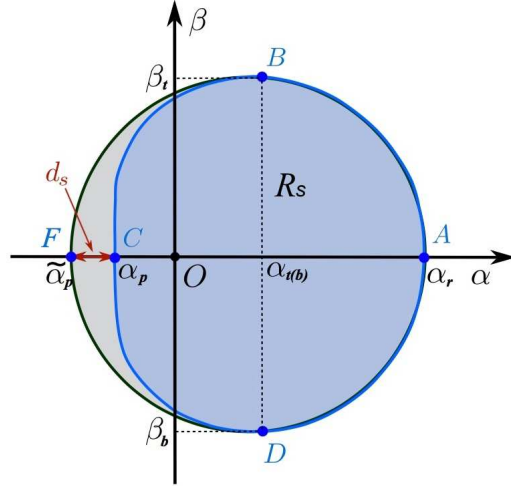


**Figure 3.** Schematic illustration of the black hole shadow and the reference circle.

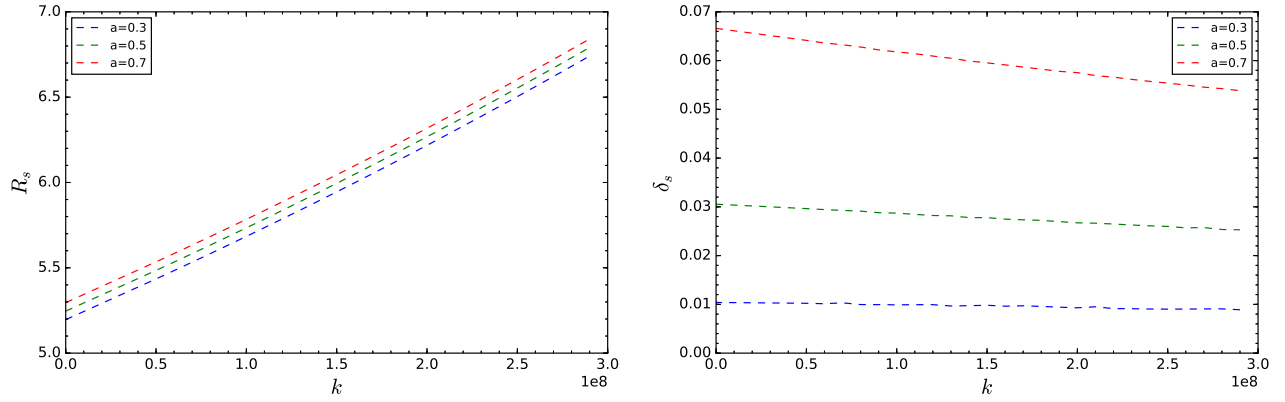


**Figure 4.** Variation of the radius  $R_s$  (left) and the distortion parameter  $\delta_s$  (right) of the shadow of Sgr A\* with the parameters  $a$  and  $k$  in the CDM halo. The lines of  $R_s$  have been moved up vertically to visualize the trend of  $R_s$  for different  $a$  by adding a constant to  $R_s$ .

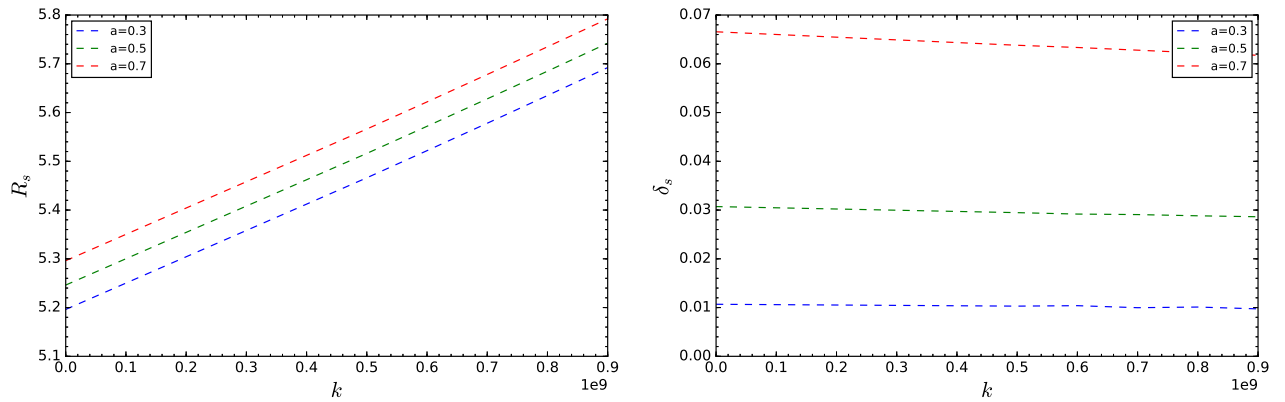


**Figure 5.** Variation of the radius  $R_s$  (left) and the distortion parameter  $\delta_s$  (right) of the shadow of Sgr A\* with the parameters  $a$  and  $k$  in the SFDM halo. The lines of  $R_s$  have been moved up vertically to visualize the trend of  $R_s$  for different  $a$  by adding a constant to  $R_s$ .

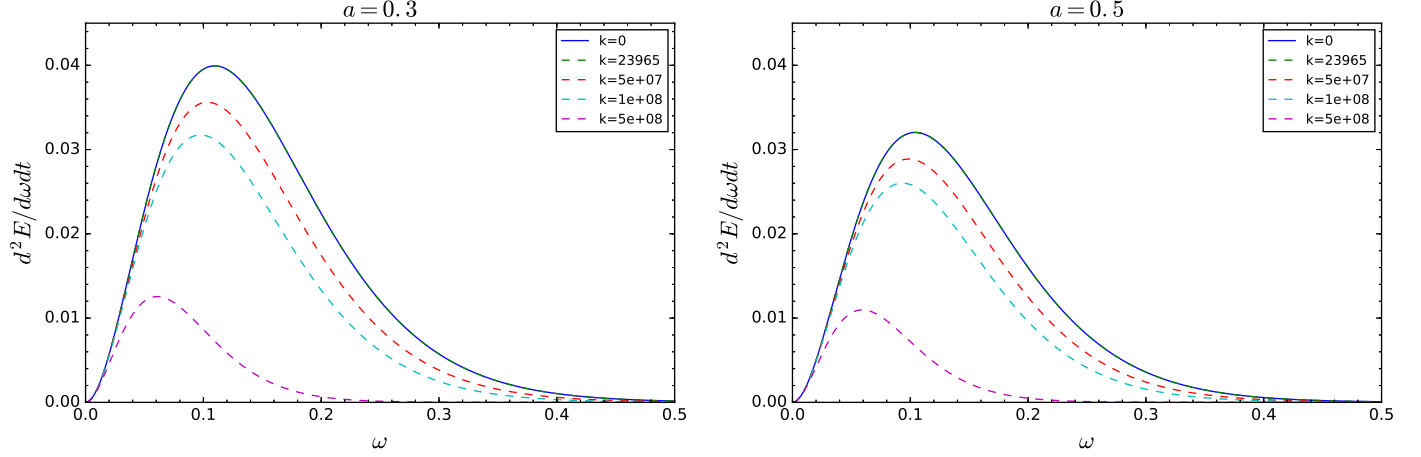


**Figure 6.** Evolution of the emission rate with the frequency  $\omega$  for different values of the parameters  $a$  and  $k$  for the CDM halo.

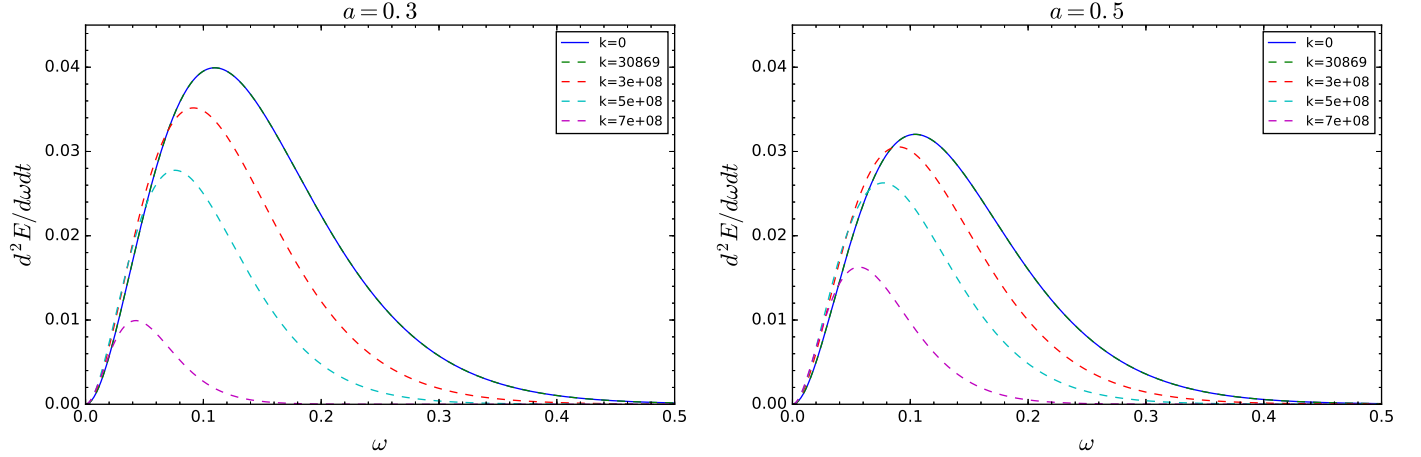


**Figure 7.** Evolution of the emission rate with the frequency  $\omega$  for different values of the parameters  $a$  and  $k$  for the SFDM halo.

with increasing  $k$  and shifts to lower frequency. Similarly, the effect of dark matter is minor and only visible when  $k$  increases to order of magnitude of  $10^7$ .

## 6. DISCUSSION

In this work, we study the shadow cast by the black hole Sgr A\* at the center of the Milky Way in dark matter halo by analysing how the shadow is influenced by the black hole spin  $a$  and the dark matter parameter  $k$ . We find that the two dark matter models (CDM and SFDM) considered in this work affect the shadow in a similar way for an observer located at infinity and in the equatorial plane. For a fixed value of  $a$ , the size of the shadow  $R_s$  increases with increasing  $k$  and the distortion parameter  $\delta_s$  monotonically decreases. For a fixed value of  $k$ , the shadow gets more and more distorted with increasing  $a$ , characterized by larger and larger  $\delta_s$ . With the assumption that the black hole shadow equals to the high energy absorption cross section, we calculate the emission rate of Sgr A\* in dark matter halo. We find that for both dark matter models, the emission rate decreases with increasing  $k$  for a fixed frequency  $\omega$  and the peak of the emission shifts to lower  $\omega$ . In general, the influence of dark matter on the black hole is minor and only becomes significant when  $k$  increases to order of magnitude of  $10^7$ , for both CDM and SFDM models.

The angular radius of the shadow can be estimated using the observable  $R_s$  as  $\theta_s = R_s M / D$ , where  $M$  is the black hole mass and  $D$  is the distance between the black hole and the observer. The angular radius can be further expressed as  $\theta_s = 9.87098 \times 10^{-6} R_s (M/M_\odot) (1 \text{ kpc} / D) \mu\text{as}$  (Amarilla & Eiroa 2012). For the supermassive black hole Sgr A\* at the center of the Milky Way, its mass is estimated to be  $M = 4.3 \times 10^6 M_\odot$  and  $D = 8.3 \text{ kpc}$  which is the distance

between the Earth and the black hole. Through calculations for  $R_s$  and  $\theta_s$ , the angular resolution required to detect the dark matter influence on the black hole shadow would be, for CDM,  $10^{-3} \mu\text{as}$  (i.e., to distinguish between  $k = 0$  and  $k = 23965$ ) and for SFDM,  $10^{-5} \mu\text{as}$  (i.e., to distinguish between  $k = 0$  and  $k = 30869$ ). This is out of the reach of the current astronomical instruments. For example, the current EHT resolution is  $\sim 60 \mu\text{as}$  at 230 GHz and will be able to achieve a finer one of  $15 \mu\text{as}$  by observing at a higher frequency of 345 GHz and adding more VLBI telescopes. The space-based VLBI RadioAstron (Kardashev et al. 2013)<sup>2</sup> will be able to obtain a resolution of  $\sim 1 - 10 \mu\text{as}$ . This is still at least three orders of magnitude lower than the resolution required by the CDM model. The angular resolution of a baseline is given by  $1/fD$ , with  $f$  the observing frequency and  $D$  the baseline which is the separation of EHT sites used for VLBI. We estimated that, for example, to achieve the resolution of  $10^{-3} \mu\text{as}$  required by the CDM model, observations at a much higher frequency of  $\sim 5 \times 10^6$  GHz or with a much longer baseline of  $\sim 4 \times 10^8$  km will be needed.

We anticipate that future observations with highly improved techniques would be able to achieve the resolution required to observe the dark matter influence on the shadow of the black hole Sgr A\*. Furthermore, the angular resolution difference between CDM and SFDM models is as large as two orders of magnitude. This implies that observing the black hole shadow of Sgr A\* may serve as a tool of distinguishing one model from the other and eventually shed light on the nature of Sgr A\* and dark matter.

We acknowledge the anonymous referee for a constructive report that has significantly improved this paper. We acknowledge the financial support from the National Natural Science Foundation of China under grants No. 11503078, 11573060 and 11661161010.

## REFERENCES

- Abdjabbarov, A., Amir, M., Ahmedov, B., & Ghosh, S. G. 2016, *Phys. Rev. D*, 93, 104004
- Abdjabbarov, A., Atamurotov, F., Dadhich, N., Ahmedov, B., & Stuchlík, Z. 2015, *European Physical Journal C*, 75, 399
- Abdjabbarov, A., Atamurotov, F., Kucukakca, Y., Ahmedov, B., & Camci, U. 2013, *Ap&SS*, 344, 429
- Abdjabbarov, A., Toshmatov, B., Stuchlík, Z., & Ahmedov, B. 2017, *International Journal of Modern Physics D*, 26, 1750051
- Amarilla, L., & Eiroa, E. F. 2012, *Phys. Rev. D*, 85, 064019
- . 2013, *Phys. Rev. D*, 87, 044057
- Amarilla, L., Eiroa, E. F., & Giribet, G. 2010, *Phys. Rev. D*, 81, 124045
- Amir, M., & Ghosh, S. G. 2016, *Phys. Rev. D*, 94, 024054
- Amir, M., Pratap Singh, B., & Ghosh, S. G. 2017, *ArXiv e-prints*, arXiv:1707.09521
- Atamurotov, F., Abdjabbarov, A., & Ahmedov, B. 2013, *Phys. Rev. D*, 88, 064004
- Atamurotov, F., Ahmedov, B., & Abdjabbarov, A. 2015, *Phys. Rev. D*, 92, 084005
- Bambi, C., Caravelli, F., & Modesto, L. 2012, *Physics Letters B*, 711, 10
- Bambi, C., & Freese, K. 2009, *Phys. Rev. D*, 79, 043002
- Bambi, C., & Yoshida, N. 2010, *Classical and Quantum Gravity*, 27, 205006
- Bardeen, J. M. 1973, in *Black Holes (Les Astres Occlus)*, ed. C. Dewitt & B. S. Dewitt, 215–239
- Broderick, A. E., Johannsen, T., Loeb, A., & Psaltis, D. 2014, *ApJ*, 784, 7
- Broderick, A. E., & Loeb, A. 2006, in *Journal of Physics Conference Series*, Vol. 54, *Journal of Physics Conference Series*, ed. R. Schödel, G. C. Bower, M. P. Muno, S. Nayakshin, & T. Ott, 448–455
- Broderick, A. E., Fish, V. L., Johnson, M. D., et al. 2016, *ApJ*, 820, 137
- Carter, B. 1968, *Physical Review*, 174, 1559
- Chan, C.-K., Psaltis, D., Özel, F., Narayan, R., & Sądowski, A. 2015, *ApJ*, 799, 1
- Cirelli, M. 2015, *ArXiv e-prints*, arXiv:1511.02031
- Cunha, P. V. P., & Herdeiro, C. A. R. 2018, *General Relativity and Gravitation*, 50, 42
- Cunha, P. V. P., Herdeiro, C. A. R., Kleihaus, B., Kunz, J., & Radu, E. 2017, *Physics Letters B*, 768, 373
- Cunha, P. V. P., Herdeiro, C. A. R., Radu, E., & Rúnarsson, H. F. 2015, *Physical Review Letters*, 115, 211102
- Cunha, P. V. P., Herdeiro, C. A. R., & Rodriguez, M. J. 2018, *ArXiv e-prints*, arXiv:1805.03798
- Dastan, S., Saffari, R., & Soroushfar, S. 2016, *ArXiv e-prints*, arXiv:1610.09477
- de Oliveira, P. L. C., de Freitas Pacheco, J. A., & Reinisch, G. 2015, *General Relativity and Gravitation*, 47, 12
- de Vries, A. 2000, *Classical and Quantum Gravity*, 17, 123
- Dexter, J., Agol, E., Fragile, P. C., & McKinney, J. C. 2010, *ApJ*, 717, 1092
- Doeleman, S. S., Weintroub, J., Rogers, A. E. E., et al. 2008, *Nature*, 455, 78
- Dubinski, J., & Carlberg, R. G. 1991, *ApJ*, 378, 496
- Eiroa, E. F., & Sendra, C. M. 2018, *European Physical Journal C*, 78, 91
- Falcke, H., Melia, F., & Agol, E. 2000, *ApJL*, 528, L13
- Goddi, C., Falcke, H., Kramer, M., et al. 2017, *International Journal of Modern Physics D*, 26, 1730001
- Gold, R., McKinney, J. C., Johnson, M. D., & Doeleman, S. S. 2017, *ApJ*, 837, 180
- Grenzebach, A., Perlick, V., & Lämmerzahl, C. 2014, *Phys. Rev. D*, 89, 124004
- Grover, J., Kunz, J., Nedkova, P., Wittig, A., & Yazadjiev, S. 2018, *ArXiv e-prints*, arXiv:1802.03062
- Harko, T. 2011, *J. Cosmology Astropart. Phys.*, 5, 022
- Hioki, K., & Maeda, K.-I. 2009, *Phys. Rev. D*, 80, 024042
- Johannsen, T., Broderick, A. E., Plewa, P. M., et al. 2016, *Physical Review Letters*, 116, 031101
- Kardashev, N. S., Khartov, V. V., Abramov, V. V., et al. 2013, *Astronomy Reports*, 57, 153
- Kumar, R., Pratap Singh, B., Sabir Ali, M., & Ghosh, S. G. 2017, *ArXiv e-prints*, arXiv:1712.09793
- Luminet, J.-P. 1979, *A&A*, 75, 228

<sup>2</sup> <http://www.asc.rssi.ru/radioastron/index.html>

- Mashhoon, B. 1973, *Phys. Rev. D*, 7, 2807
- Misner, C. W., Thorne, K. S., & Wheeler, J. A. 1973, *Gravitation*
- Mizuno, Y., Younsi, Z., Fromm, C. M., et al. 2018, *Nature Astronomy*, arXiv:1804.05812
- Mościbrodzka, M., Falcke, H., Shiokawa, H., & Gammie, C. F. 2014, *A&A*, 570, A7
- Mureika, J. R., & Varieschi, G. U. 2017, *Canadian Journal of Physics*, 95, 1299
- Navarro, J. F., Frenk, C. S., & White, S. D. M. 1996, *ApJ*, 462, 563
- . 1997, *ApJ*, 490, 493
- Noble, S. C., Leung, P. K., Gammie, C. F., & Book, L. G. 2007, *Classical and Quantum Gravity*, 24, S259
- Olive, K. A. 2003, *ArXiv Astrophysics e-prints*, astro-ph/0301505
- Papnoi, U., Atamurotov, F., Ghosh, S. G., & Ahmedov, B. 2014, *Phys. Rev. D*, 90, 024073
- Perlick, V., Tsupko, O. Y., & Bisnovatyi-Kogan, G. S. 2015, *Phys. Rev. D*, 92, 104031
- . 2018, *ArXiv e-prints*, arXiv:1804.04898
- Planck Collaboration, Ade, P. A. R., Aghanim, N., et al. 2014, *A&A*, 571, A16
- Pratap Singh, B. 2017, *ArXiv e-prints*, arXiv:1711.02898
- Pratap Singh, B., & Ghosh, S. G. 2017, *ArXiv e-prints*, arXiv:1707.07125
- Psaltis, D., Özel, F., Chan, C.-K., & Marrone, D. P. 2015, *ApJ*, 814, 115
- Rubin, V. C., Ford, Jr., W. K., & Thonnard, N. 1980, *ApJ*, 238, 471
- Saha, A., Modumudi, M., & Gangopadhyay, S. 2018, *ArXiv e-prints*, arXiv:1802.03276
- Schee, J., & Stuchlík, Z. 2009, *International Journal of Modern Physics D*, 18, 983
- Spergel, D. N., & Steinhardt, P. J. 2000, *Physical Review Letters*, 84, 3760
- Synge, J. L. 1966, *MNRAS*, 131, 463
- Takahashi, R. 2005, *PASJ*, 57, 273
- Tsukamoto, N. 2018, *Phys. Rev. D*, 97, 064021
- Tulin, S., & Yu, H.-B. 2018, *Phys. Rep.*, 730, 1
- Ureña-López, L. A., Matos, T., & Becerril, R. 2002, *Classical and Quantum Gravity*, 19, 6259
- Vetsov, T., Gylchev, G., & Yazadjiev, S. 2018, *ArXiv e-prints*, arXiv:1801.04592
- Wang, M., Chen, S., & Jing, J. 2017, *J. Cosmology Astropart. Phys.*, 10, 051
- Wei, S.-W., & Liu, Y.-X. 2013, *J. Cosmology Astropart. Phys.*, 11, 063
- Xu, Z., Hou, X., Gong, X., & Wang, J. 2018, *ArXiv e-prints*, arXiv:1803.00767
- Younsi, Z., Zhidenko, A., Rezzolla, L., Konoplya, R., & Mizuno, Y. 2016, *Phys. Rev. D*, 94, 084025
- Yumoto, A., Nitta, D., Chiba, T., & Sugiyama, N. 2012, *Phys. Rev. D*, 86, 103001
- Zwicky, F. 1933, *Helvetica Physica Acta*, 6, 110